CHEMPHYSCHEM

DOI: 10.1002/cphc.201000913

Davydov Splitting of Excitons in Cyclic Bacteriochlorophyll *a* Nanoaggregates of Bacterial Light-Harvesting Complexes between 4.5 and 263 K

Mihkel Pajusalu,[a] Margus Rätsep,[a] Gediminas Trinkunas,[b] and Arvi Freiberg*[a, c]

The nature of electronic excitations created by photon absorption in the cyclic B850 aggregates of 18 bacteriochlorophyll molecules of LH2 antenna complexes of photosynthetic bacteria is studied over a broad temperature range using absorption, fluorescence, and fluorescence anisotropy spectra. The latter technique has been proved to be suitable for revealing the hidden structure of excitons in inhomogeneously broadened spectra of cyclic aggregates. A theoretical model that accounts for differences of absorbing excitons in undeformed and emitting exciton polarons in deformed antenna lattices is also developed. Only a slight decrease of the exciton bandwidth and exciton coupling energy with temperature is observed. Survival of excitons in the whole temperature span from cryogenic to nearly ambient temperatures strongly suggests that collective, coherent electronic excitations might play a role in the functional light-harvesting process taking place at physiological temperatures.

1. Introduction

Nanoscale systems structurally link molecular and bulk materials. A natural question then arises: Are their electronic properties also intermediate to those of the molecules and bulk systems? This fundamental question, although addressed,[1,2] attracted relatively little attention until the last decade. Since then, there has been an explosive wake of interest in quantum aggregates due to the advent of refined experimental procedures with which to study and fabricate nanoscale molecular structures of great potential technical importance. Notable examples include plastic electronics and photonics, organic solar cells, fluorescent (bio)markers, and artificial photosynthesis systems (see refs. [3–8] for reviews). The surplus of various applications underlines the importance of studying the fundamental properties of the molecular quantum aggregates. A well-founded general prospect is that on the nanoscale the solid-state materials acquire molecular-like spectroscopic features, first of all discrete transitions.[1,2] The aggregate formation is frequently accompanied by rather spectacular changes in optical properties whose origin is a coherent excitation extending over many monomers—an exciton. The idealized exciton states interact with local vibrations of the monomers themselves and of the collective vibrations (phonons) of the surroundings, leading to electron–vibration and electron–phonon couplings, respectively. As such the molecular aggregates are expected to form model objects with which to study the effects of decoherence and dissipation of the coherent electronic excitations. Yet the real nanosamples often suffer from inhomogeneous composition in terms of structural and spectral disorder as well as from size polydispersity.[4–6] For this reason, even the spread of the discrete exiton state manifold, holding the all-important information about exciton coupling energy, is difficult to estimate.

Herein, we take advantage of studying molecular quantum aggregates of biological origin where the inner biological machinery uniquely controls the composition and size of the aggregates. Great variety of natural biological quantum aggregates are available[9] that include from about 10000 (as in chlorosomes[10]) to 2 (encountered as a basic structural motif in many (bacterio)chlorophyll light-harvesting systems[9,11–13]) molecules. Absence of size dispersion and diversity of available genetic manipulation techniques makes these samples particularly attractive. The samples that suite best for the purpose of the present work are cyclic aggregates of bacteriochlorophyll *a* (Bchl) molecules found in light-harvesting (LH) pigment–protein complexes of purple photosynthetic bacteria.[11,14,15] These membrane proteins harvest solar photons and transfer the resulting excitation energy to the reaction centers, where it is transformed into potential chemical energy. Excitons, or rather exciton polarons (excitons coupled to lattice vibrations), have long been recognized in the bacterial LH complexes as primary excitations created by solar light absorption (see ref. [11] for a review). The excitons can decay radiatively giving rise to fluorescence. In native conditions, the antenna excitons quickly

[a] *M. Pajusalu, Dr. M. Rätsep, Prof. A. Freiberg*
Institute of Physics
Tartu University, Riia 142, Tartu 51014 (Estonia)
Fax: (+372) 73 83 033
E-mail: arvi.freiberg@ut.ee

[b] *Dr. G. Trinkunas*
Center for Physical Sciences and Technology
Savanoriu 231, LT-02300 Vilnius (Lithuania)

[c] *Prof. A. Freiberg*
Institute of Molecular and Cell Biology
Tartu University, Riia 23, Tartu 51010 (Estonia)

Supporting information for this article is available on the WWW under http://dx.doi.org/10.1002/cphc.201000913.

move along the photosynthetic energy transfer pathways, thus limiting the quantum yield of fluorescence.[16–19] For purified LH complexes, however, fluorescence is a predominant channel of excitation decay, being easily observable. In a variety of wild-type purple bacteria the photosynthetic apparatus is organized into chromatophore vesicles of nearly spherical shape of 50–60 nm diameter[20] that are mainly populated by core LH1 and peripheral LH2 antenna complexes. High-resolution structural models for the LH complexes have also been known for some time for a number of species. Here, we focus on the peripheral LH2 antenna complex, by far the most studied and best-characterized photosynthetic light-harvesting system reviewed in refs. [11, 14, 15, 21] The basic building block of the cyclic LH2 structure is a heterodimer of α-helical α- and β-apoproteins, each non-covalently binding three Bchl molecules. There are nine of such αβ-heterodimers in LH2 from *Rhodopseudomonas (Rps.) acidophila*, forming a dimerized ring of nearly 6 nm diameter. A remarkable feature of the organization of the 27 Bchl molecules in LH2 is their partition into two concentric pools. Eighteen of the Bchl molecules present a ring of overlapping Bchls in a water-wheel arrangement. The other 9 pigments in the cytoplasmic side of the membrane are more loosely packed. The latter molecules also have their bacteriochlorin planes oriented perpendicular to the symmetry axis of the protein. This is the tightly packed, 18-member cyclic molecular aggregate that is the main interest of this work.

Spectroscopic properties of the LH2 complexes have been extensively studied both in bulk solutions and as single surface-immobilized molecules (see [15, 21–23] for reviews). While free in organic solvents, the lowest singlet electronic transition of Bchl (denoted as the Q_y transition) is located in the near-infrared optical region at ~770 nm. The pigments in the 18-member ring of the LH2 complex, however, give rise to absorption around 850 nm (that is why this absorption band is universally called the B850 band, Figure 1 a). This huge, almost 100 nm red-shift essentially arises from a combined effect of the interactions between transition densities of the Bchl molecules (resulting in an exciton shift component) and between each Bchl and its surrounding protein (a solvent/protein shift). Universal dispersion couplings aside, specific factors that mostly contribute into the latter shift are hydrogen bonding, axial ligation, and various conformational interactions. An exciton origin of the B850 ground-state absorption spectrum can be well recognized by comparing it with the distribution of the exciton states (DOS). Both the absorption spectrum and DOS as presented in Figure 1 b are calculated according to the simple disordered Frenkel exciton model[24] that does not account for exciton–phonon couplings. As can be seen from this figure, the absorption and DOS spectra are qualitatively different. While the exciton states are spread over a significant spectral span, the optically allowed states appear mostly at the low-energy edge of the distribution. The upper exciton components are represented by just a weak absorption shoulder around 770 nm. Uneven distribution of DOS is also worth noticing. Due to dimeric structure of the Bchl chain imposed by the surrounding protein scaffold, the exciton states are partitioned into two sub-groups, 9 states in each sub-group.[24, 25] In

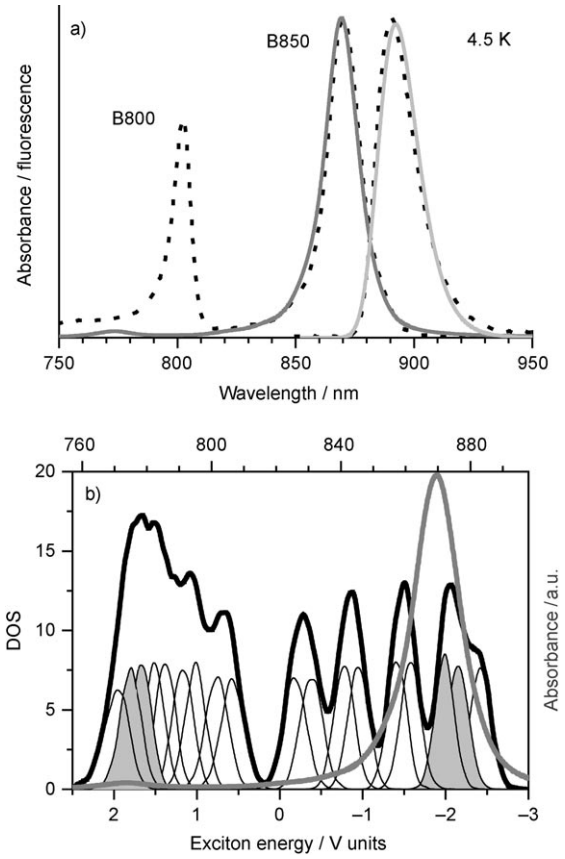

Figure 1. a) Experimental (dashed lines) and simulated low-resolution absorption (dark gray line) and fluorescence emission (light gray line) spectra of LH2 antenna complexes from *Rps. acidophila* at 4.5 K. In the experimental absorption spectrum two distinct peaks are visible. A high-energy peak around 800 nm (denoted as B800) is related to the absorbing states of the B800 ring of Bchl molecules, while the low-energy peak around 870, by the B850 ring. The simulated spectra represent just the tightly coupled B850 aggregate ensemble averages. b) The calculated absorption spectrum (grey bold line) and the corresponding DOS (black bold line) for an ensemble of 2000 B850 aggregates. The shapes drawn with thin black line represent ensemble distributions of 18 individual exciton states ($k = 0, \pm 1, \pm 2, \ldots, \pm 8, 9$, as counted from the low-energy side). The filled grey areas highlight the distributions for the disorder-split $k = \pm 1$ and $k = \pm 8$ exciton states. The exciton energy scale is given in the units of the nearest-neighbor coupling energy, *V*. See text for further detail.

molecular crystal theory terminology,[26] one would talk about two molecules in a unit cell and about two Davydov sub-bands, respectively. Splitting between the Davydov sub-bands is a measure of exciton coupling energy as well as of exciton bandwidth in crystals.

Unfortunately, the optical transitions corresponding to the lower and upper edges of the B850 exciton band (the $k = 0$ and $k = 9$ excitons, respectively[11, 15]) are both very weak (see Figure 1 b). This weakness is the prime result of the special arrangement of the Bchl molecules in this aggregate.[27] Disorder averaging and overlap with the strong B800 absorption and a background absorbance of detached Bchl chromophores that always present in the system[28] further complicate the situation. These physical constraints make it practically impossible to evaluate the bandwidth of the B850 excitons from linear ab-

sorption. Fortunately, it has been demonstrated[29,30] that a fluorescence anisotropy excitation spectroscopy is able to reveal hidden structures of exciton bands in the cyclic molecular aggregates. In particular, two fluorescence anisotropy minima were discovered that correlated with the exciton band boundaries. This way the bandwidths of exciton state manifolds in LH1, LH2, and LH3 antenna complexes from various bacterial species were estimated.[23,29–31] Some of these results were confirmed by alternative methods.[32] Although polarization properties of excitons in LH complexes, being primary governed by the ring-shape symmetry of the B850 aggregate and by specific orientation of the transition dipole moments with respect to the ring plane, vary from those in three-dimensional crystals, one can still establish a formal connection between them by identifying the energy difference between the fluorescence anisotropy dips as Davydov splitting.

The objective of this work is to study survival of excitons in the B850 aggregates of LH2 antenna complexes from the photosynthetic bacterium *Rps. acidophila* upon increase of temperature. This particular sample was selected due to the availability of the precise atomic structure of the complex.[27] We want to understand whether coherent collective electronic excitations play any role in the light-harvesting process at physiological temperatures. An attempt is thus undertaken to bridge a long-standing gap between molecular biology and quantum physics in the area of photosynthetic light harnessing. To achieve this goal, temperature dependence of the exciton bandwidth (termed in the title as Davydov splitting) in B850 aggregates was followed over a wide temperature range spanning from the boiling point of liquid He to nearly ambient temperature of 263 K. The behavior of conventional absorption and fluorescence emission spectra was also studied in the same temperature range. A quantum mechanical model of the B850 aggregate was constructed that well reproduced all major experimental observations. Aspects of the B850 excitons as a function of temperature have been studied before.[33–38] However, this is the first time that temperature dependence of the Davydov splitting (thus the exciton coupling energy) is studied for any structurally well-defined molecular nanoaggregate.

2. Results and Discussion

2.1. Experimental Results

The absorption and fluorescence emission spectra of the LH2 complexes at 4.5 K are shown in Figure 1a by dashed lines. The two peaks in the absorption spectrum at 802.2 and 870.4 nm are related to the B800 and B850 chromophore rings, which in the intact photosynthetic membrane are located at opposite sides of the membrane. Since herein we are mostly concerned with the aggregate of chromophores responsible for the strong absorption around 870 nm, in the modeled (see below for modeling detail) absorption and fluorescence emission spectra drawn in Figure 1a with dark and light gray lines, respectively, the B800 peak is missing.

Figure 2 demonstrates the fluorescence anisotropy spectrum measured at 4.5 K (scattered line) and the reference absorption

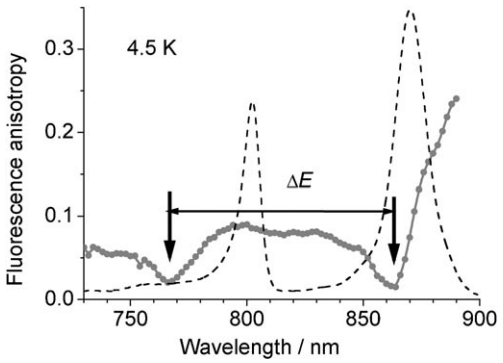

Figure 2. Fluorescence anisotropy excitation spectrum of LH2 complexes from *Rps. acidophila* measured at 4.5 K (scattered line). Arrows indicate the positions of the two minima discussed in the text. The absorption spectrum on the background drawn with dashed line is shown for reference.

spectrum (dashed line). The scattered laser line was subtracted from the fluorescence emission spectrum and full intensity of the emission in the range of 840–940 nm was used for calculating the anisotropy according to Equation (14) below. In agreement with the earlier measurements,[23,29–31] the anisotropy is generally low, around 0.07, at excitation wavelengths shorter than the B850 absorption maximum. Toward longer wavelengths the anisotropy rapidly increases, approaching a theoretical limit of 0.4. As noticed first by Timpmann et al.,[29] in the low-anisotropy range there is a noticeable structure with two minima. The slightly narrower and deeper minimum at about 862 nm may be connected to the main absorption peak at 870.4 nm. The broader and lower minimum at about 766 nm is apparently not correlated with any structure of the absorption spectrum. However, comparison with the simulated absorption spectrum shown in Figure 1 strongly suggests that the high-energy minimum could be related to the upper edge of the excition band. In analogy with the former works,[23,29–31] we thus tentatively assign the low-energy anisotropy minimum at 862 nm to the strongly absorbing exciton components with $k=\pm 1$, whilst the high-energy minimum at 766 nm, to the weak exciton components with $k=\pm 8$. Their energy difference is further called the energy gap, ΔE, and operationally identified with the exciton bandwidth. It is of notice that no structure of the anisotropy spectrum correlates with the B800 absorption band. This underscores insignificant exciton coupling between the photo-excitations in the two pigment rings of LH2 complexes, in agreement with earlier observations.[39]

Figure 3 shows temperature dependence of the anisotropy spectra measured for the LH2 complexes from *Rps. acidophila* in the temperature range from 4.5 to 263 K. As can be seen from this figure, the two anisotropy minima discussed above demonstrate vastly different sensitivity to rising temperature in terms of their position and width. While the low-energy dip at 11 605 cm^{-1} (as of the 4.5 K value) rapidly and extensively (by 180 cm^{-1}) shifts to the blue side of the spectrum and practically disappears at near ambient temperatures, the high-energy minimum at 13 045 cm^{-1} is fairly indifferent to temperature. Over the whole temperature range it shifts to lower energies only by ~10 cm^{-1}, its depth diminishing roughly by a factor of

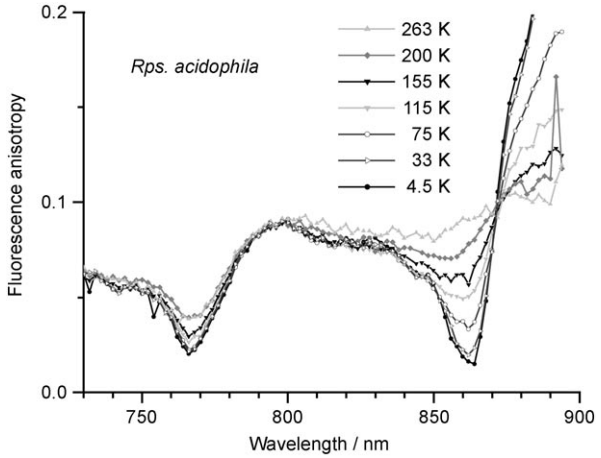

Figure 3. The effect of temperature on fluorescence anisotropy excitation spectra of LH2 complexes from *Rps. acidophila*.

two. Because of the shift rate differences of the two dips, the gap gradually decreases with temperature, as demonstrated in Figure 4. Total narrowing of the experimental gap is 183 cm^{-1} (from 1442 cm^{-1} at 4.5 K to 1259 cm^{-1} at 263 K), which, considering the size of the gap at low temperature is rather minor (~13%). We also notice that almost all of this gap change is produced in the high temperature interval above ~100 K; below 100 K the gap is practically constant.

To explain the temperature dependence of absorption spectra of LH2 complexes of *Rps. acidophila*, an increase by about

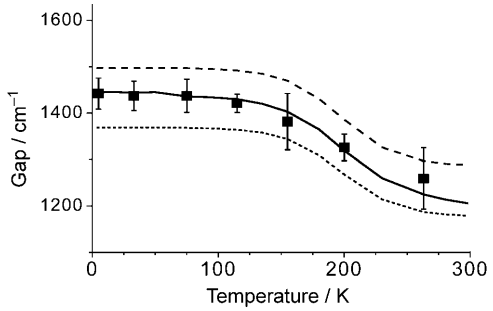

Figure 4. Experimental (black squares with error bars) and simulated (solid line) energy gap values of LH2 complexes from *Rps. acidophila* as a function of temperature. The dashed and dotted lines indicate energy difference between the $k=0$ and $k=9$, and $k=\pm1$ and $k=\pm8$ exciton states, respectively.

35% of the exciton coupling energy with lowering temperature in the 100–200 K range was suggested.[36] Although the increase of exciton couplings projected in ref. [36] was much bigger than found here, the results of Figure 4 may be regarded as a qualitative confirmation of this former insight. A twice decrease of compressibility of the LH2 complexes from *Rhodobacter* (*Rb.) sphaeroides* has also been observed,[40] in association with a phase transition in the protein-buffer–glycerol mixed solution at 156 K. Thermal contraction is the plausible common physical mechanism that explains both the tightening of the protein structure and the increase of exciton interactions upon cooling.

To get further insights into temperature dependence of the anisotropy spectra, the absorption and fluorescence emission spectra of the LH2 complexes from *Rps. acidophila* were studied over similar broad temperature range. The outcome of these measurements, parallel to that obtained by former researches,[33–37] is presented in Figures 5 a,b for absorption and fluorescence, respectively. There is substantial blue-shift and broadening of both spectra with temperature. However, the

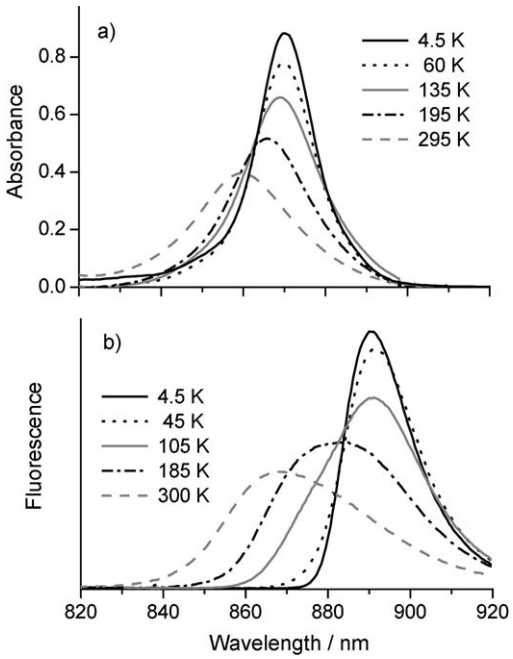

Figure 5. Experimental a) absorption and b) fluorescence emission spectra of LH2 complex from *Rps. acidophila* as a function of temperature.

temperature-induced changes in fluorescence spectra are more significant. The overall shift (260 cm^{-1}) of the emission spectrum is twice bigger than that of the absorption spectrum (130 cm^{-1}), which causes diminishing of the Stokes shift with temperature. Furthermore, the emission spectrum, being broader than the absorption spectrum at 4.5 K (245 cm^{-1} versus 210 cm^{-1}) also broadens faster upon heating the sample. The qualitatively different temperature dependencies of the absorption and fluorescence emission spectra can be more clearly followed in Figure 6, where the spectral positions and bandwidths in respective spectra are directly compared. Please notice that here and below, the line widths are customarily determined as full widths at half maximum height.

2.2. Theoretical Aspects

According to the current wisdom, excitations within the B850 aggregate ring are Frenkel excitons spreading between several $\alpha\beta$ protein subunits. The Frenkel exciton states thus participate in absorption of energy by the aggregate during photo-excitation. Delocalization of the photo-excitation lowers energy of

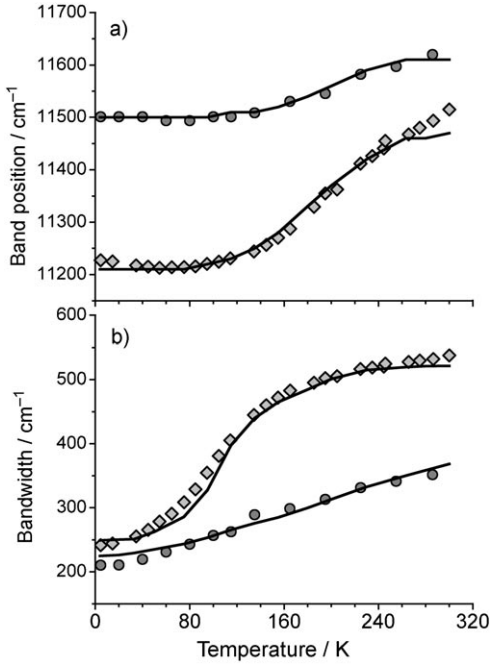

Figure 6. Temperature dependence of the B850 absorption and fluorescence emission peak positions (a) and bandwidths (b) in LH2 complexes from *Rps. acidophila*. The experimental data in absorption and fluorescence emission spectra are depicted with circles and diamonds, respectively. Solid lines follow the corresponding simulated values.

the system by twice the electronic coupling strength. The inter-pigment interactions that cause this coherence also produce the splitting of the exciton energy states. These states are commonly labeled with the quantum numbers $k = 0, \pm 1, \pm 2, \ldots, \pm 8,9$ (in increasing energy order). In a perfectly ordered, symmetrical system the $\pm$ states are pairwise degenerate, whilst in realistic, statically and/or dynamically disordered systems the degeneracy is removed, creating 18 energetically different states. Interactions of Frenkel excitons with the quanta of local vibrations and/or delocalized phonons form new quasiparticles—the excitons clothed by a phonon cloud or exciton polarons. The phonon cloud can be thought about as a distortion of the local environment around an electronically excited chromophore. It forces the exciton to slow down and further lowers the system's energy.[8,41–45]

Dynamic aspects of photo-excitations in the LH2 antenna have been studied in a great number of experimental and theoretical works.[22,23,33,34,40,46–56] For theory, when aiming at simultaneously description of the steady state absorption and fluorescence emission spectra in wide temperature range, the greatest challenge is dealing with the exciton and exciton–bath couplings of similar magnitude.[35,37] As follows, the simplest model of absorbing and emitting states in the B850 aggregate is introduced. It assumes identical dynamic broadening of all the absorbing exciton states caused by diagonal exciton-phonon bath coupling. The required extra lowering of the fluorescing states[35] is introduced by the Su–Schrieffer–Heeger (SSH) or nonlocal polaronic coupling mechanism (reviewed in ref. [57]).

Absorbing Frenkel Exciton States

As previously mentioned, there are $N = 18$ excitonically interacting pigment sites n within the B850 ring. The rigid-lattice Hamiltonian for a disordered Frenkel exciton system can be written in a site representation as Equation (1):

$$H_0 = \sum_{n=1}^{N} (\varepsilon_0 + \delta\varepsilon_n)|n\rangle\langle n| + \sum_{n,m=1;n\neq m}^{N} (t_m + \delta t_{nm})|n\rangle\langle m| \quad (1)$$

Here, ε_0 is the average site energy, t_{nm} are the mean off-diagonal elements of the coupling matrix, $\delta\varepsilon_n$ represents the diagonal disorder (disorder of static and dynamic displacement energies) and δt_{nm}, the off-diagonal disorder (disorder in structure). t_{nm} can be calculated knowing the structure of the system[58] (see the Supporting Information). However, due to the fact that the effects of off-diagonal and diagonal disorder on Frenkel excitons have been proven to be indistinguishable to certain extent,[59] in the following, we only apply diagonal disorder, modeled using a Gaussian probability distribution function with standard deviation of σ [Eq. (2)]:

$$P(\delta\varepsilon) = \frac{1}{\sqrt{2\pi\sigma^2}} \exp\left(-\frac{\delta\varepsilon^2}{2\sigma^2}\right) \quad (2)$$

The energy spectrum and dipole moments of the exciton-coupled system can be obtained by solving an eigenvalue problem for the Hamiltonian [Eq. (1)] in a dipole–dipole approximation [Eq. (3)]:

$$\sum_{m=1}^{N} \langle n|H_0|m\rangle a_{mk} = E_k^f a_{nk} \quad (3)$$

where a_{nk} is the collection of the system's eigenvectors and E_k^f are the eigenenergies of the corresponding absorbing Frenkel excitons. In Equation (3), the upper index f refers to the Frenkel excitons and the lower index k, to the wave vector that is related to the crystal momentum $\hbar k$.

The system's eigenfunctions are then obtained as Equation (4):

$$|k\rangle = \sum_{n=1}^{N} a_{nk}|n\rangle \quad (4)$$

The participation factor of individual molecular states n in the Frenkel exciton state k is given by Equation (5):

$$p_k^f = \sum_{n=0}^{N} a_{nk}^4 \quad (5)$$

Homogeneous broadening of the Frenkel exciton states is described by the diagonal exciton–phonon bath coupling,[60] assuming the same spectral density function (SDF) for each molecule of the B850 ring. Its parametric form used in numerical calculations is given by Equation (6):[35,37,58]

$$C(\omega) = \sum_{n=1}^{2} \omega^{n+1} \cdot \exp\left(-\frac{\omega}{\omega_{cn}}\right) \cdot \frac{\alpha_n}{(n+1)! \cdot \omega_{cn}^n} \quad (6)$$

where α_n are the relative constants of the local coupling to the bath[58] and ω_{cn} the characteristic frequencies. These parameters have been adapted from the experimental line-shape studies.[52,53,61]

SDF defines the reorganization energy of the system [Eq. (7)]:

$$\lambda_0 = \int_0^\infty \frac{1}{\omega} \cdot C(\omega) d\omega \quad (7)$$

as well as the line shape broadening function $g(t)$ [Eq. (8)]:[62]

$$g(t) = \int_{-\infty}^{\infty} d\omega \frac{C(\omega)}{\omega^2} \{\Theta_T[1 - \cos(\omega t)] + i[\sin(\omega t) - \omega t]\} \quad (8)$$

where $\Theta_T = \coth(\hbar\omega/2k_BT)$ (k_B is the Boltzmann constant).

With the help of $g(t)$, one can write down the timescale form of the absorption spectrum, $S_k^f(t)$, for the absorbing Frenkel exciton state k [Eq. (9)][37]

$$S_k^f(t) = D_k^f \exp\left(-g(t)p_k^f - itE_k^f - \gamma^e|t|\right) \quad (9)$$

where D_k^f is the square of the transition dipole moment of the kth Frenkel exciton state and γ^e represents lifetime broadening of the state modeled by a Lorentzian distribution. γ^e is independent of k, that is, broadenings due to relaxation of Frenkel exciton states into self-trapped exciton states are considered identical for all k. The Fourier transform of $S_k^f(t)$ is the absorption spectrum, $S_k^f(\omega)$.

A single complex spectrum is obtained when the spectra of all the k states are summed up. The spectrum of a macroscopic sample, consisting large number of complexes, can be calculated using the Monte Carlo procedure for generating spectra of single realizations of internal diagonal disorder σ. By summing together the spectra of different realizations, the ensemble spectrum is achieved. To simulate external disorder as defined in refs. [24,63], the result can be convoluted with another inhomogeneous distribution function (also modeled by a Gaussian distribution) with a standard deviation of σ_{ext}. As seen below, we allow σ_{ext} to be different for absorbing and emitting states.

Emitting Exciton Polaron States

According to the SSH model,[57] the Hamiltonian for the thermalized (relaxed) emitting states can be built by augmenting the Hamiltonian with the lattice deformation energy [Eq. (10)]:

$$H = H_0 + c\sum_n (q_n - q_{n-1})(|n\rangle\langle n+1| + |n+1\rangle\langle n|) + \frac{1}{2}\sum_n (q_n - q_{n-1})^2 \quad (10)$$

Here, q_n is the local lattice distortion at site n and c is the nonlocal coupling constant of the exciton–distortion interaction used as a free fitting parameter. The corresponding Schrödinger equation is nonlinear, but a solution can be found using an iterative procedure.[64] When the eigenfunctions and the eigenenergies of the exciton polaron states are known, the rest of the physical characteristics can be calculated as in the case of the Frenkel excitons.

For the moderate homogeneous broadening the mirror symmetry relation for the line shape function can be applied when simulating the fluorescence spectrum [Eq. (11)]:[60]

$$S_k^p(t) = D_k^p \exp\left(-\bar{g}(t)p_k^p - itE_k^{p'} - t|\gamma^p|\right) \quad (11)$$

In (11), D_k^p is the dipole strength of the kth exciton polaron state, p_k^p is the participation factor for the polaron (p) state k, defined analogous to Equation (5), and $E_k^{p'}$ denotes the shifted position of the complex conjugate lineshape of the fluorescence spectrum. It is related to the exciton polaron state energy E_k^p (generally different from E_k^f due to the exciton–phonon coupling-induced exciton autolocalization) as Equation (12):

$$E_k^{p'} = E_k^p - 2\lambda_0 p_k^p \quad (12)$$

We note that in the current model we use identical phonon baths for both absorbing and emitting states, and the absorption/emission line shapes are complex conjugates.

At zero temperature the only emitting exciton polaron state is the state with the lowest energy. When temperature rises, thermally assisted energy transfer to higher exciton polaron states (that correspond to the given lattice distortion) may occur. Thermal occupation of the higher exciton polaron states can be modeled by weighing them with Boltzmann factors when summing together the spectra of single states to form the complete fluorescence spectrum of the B850 aggregate [Eq. (13)]:

$$S_\Sigma^p(\omega) = \sum_{k=1}^{N} S_k^p(\omega) \exp\left(-\frac{E_k^p - E_0^p}{k_BT}\right) \quad (13)$$

Fluorescence Anisotropy Spectrum

The anisotropy spectrum ties together microscopic angles α_k between the absorbing end emitting states and the macroscopic polarization spectra $r(\omega)$, $r(\omega) = \langle(3\cos\alpha_k - 1)/5\rangle$, where the broken brackets denote ensemble averaging and ω is the frequency of the excitation light. $r(\omega)$ can be evaluated as Equation (14):

$$r(\omega) = \frac{I_{vv}(\omega) - I_{vh}(\omega)}{I_{vv}(\omega) - 2I_{vh}(\omega)} \quad (14)$$

where $I_{vv}(\omega)$ and $I_{vh}(\omega)$ are the integrated fluorescence intensities polarized, respectively, in parallel (index vv) and perpendicular (vh) with the vertically linearly polarized excitation light.[65]

The integral emission from a pair of the k and n states [one of which is absorbing (f) and the other one is emitting (p)] can be written as Equation (15):[23]

$$I_{kn}(\omega) = S_k^f(\omega) D_k^f D_n^p \quad (15)$$

When combining the two previous equations and summing over all emitting and absorbing states (the emitting states are summed using Boltzmann factors as previously indicated), one can find the integral fluorescence spectra at a given frequency for both experimental polarizations [Eqs. (16) and (17)]:

$$I_{vv}(\omega) = \sum_{k=1}^{N} \left[S_k^f(\omega) D_k^f \sum_{n=1}^{N} (1 + 2r_{kn}) D_n^p \exp\left(-\frac{E_k^p - E_0^p}{k_B \cdot T} \right) \right] \quad (16)$$

$$I_{vh}(\omega) = \sum_{k=1}^{N} \left[S_k^f(\omega) D_k^f \sum_{n=1}^{N} (1 - r_{kn}) D_n^p \exp\left(-\frac{E_k^p - E_0^p}{k_B \cdot T} \right) \right]. \quad (17)$$

In these equations, the factor r_{kn} represents the microscopic anisotropy between the states k and n [Eq. (18)]:

$$r_{kn} = \frac{3 \frac{\left|\mu_k^f \cdot \mu_n^p\right|}{\left|\mu_k^f\right| \left|\mu_n^p\right|} - 1}{5}. \quad (18)$$

Here, $\mu_k^f$and μ_k^p are the dipole vectors of the kth absorbing Frenkel exciton state and the nth emitting exciton–polaron state. When the polarized integral fluorescence excitation spectra for all the complexes are known, the macroscopic anisotropy from the sum of those spectra can be calculated using Equation (18).

2.3. Simulations of the Experimental Spectra

The simulations cover the whole set of the experimental data, which include absorption, fluorescence emission, and fluorescence emission anisotropy spectra as well as their temperature dependences over the full studied temperature range. The aim of these simulations is to verify the above theoretical model and to evaluate numerical values of the model parameters. Equations (8), (13), (16), and (17) reflect theoretical temperature dependences of the spectra. Higher thermal sensitivity of the fluorescence spectrum as compared to the absorption spectrum was noted. This is expected because of emerging emission from the higher exciton polaron states populated by temperature and modeled according to Equation (13). Yet, as our preliminary trials showed, the above equations fail to reproduce experimental dependences at higher temperatures past about 100 K. Obviously, additional mechanisms are involved that cause extra broadening and shift of the spectra at these high temperatures. In relation with the results of refs. [36, 40], we assign this mechanism to thermal expansion of the LH2 complexes. Empirical Equation (19) (see the Experimental Section) is developed to describe this dependence.

The applied iterative fitting procedure begins with simulations of the absorption and emission spectra at low temperatures. It continues with modeling of the temperature dependencies of the spectra. Further refinement of the parameters is achieved with fitting of the anisotropy spectra at different temperatures, thus concluding the first round of the simulations. The same routine is repeated all over again with adjusted parameters until satisfactory results are achieved. Some of the best-fit parameters evaluated from the simulations are listed in Table 1. A uniform lifetime broadening equal to 80 cm^{-1} of the Frenkel exciton states (similarly, of the unrelaxed exciton polaron states) is applied, whereas the width of the exciton polaron ground state is related to the 1–2 ns lifetime of the LH2 fluorescence emission.[23,29–31] As follows the best-fit simulation records are briefly discussed.

Table 1. Model parameters.

Parameter		Value	Unit
ω_{c1}	Frequency of the first component of the SDF	51	cm^{-1}
ω_{c2}	Frequency of the second component of the SDF	15	cm^{-1}
α_1	Weight of the first component of SDF	8.0	
α_2	Weight of the second component of SDF	15.8	
ν_0	Transition energy in non-interacting system	12279	cm^{-1}
		814.4	nm
Δ	Energy difference of the dimerized sites	306	cm^{-1}
σ	Standard deviation of diagonal disorder distribution (internal disorder)	160	cm^{-1}
σ_{exta}	External disorder for absorbing states	11	cm^{-1}
σ_{exte}	External disorder for emitting states	46	cm^{-1}
$c^2/2$	Reorganization energy of the off-diagonal exciton-distortion coupling, Equation (10)	73	cm^{-1}
λ_0	Reorganization energy for diagonal exciton-phonon bath coupling	285	cm^{-1}
V	Nearest neighbor exciton coupling strength	374 (5 K) 322 (300 K)	cm^{-1}

The simulated absorption and fluorescence emission spectra at 4.5 K are presented with solid lines in Figure 1. The fits are reasonable since the simulated spectra only slightly deviate from the measured spectra. The divergence mostly concerns the fluorescence spectrum, the simulated curve being a bit narrower and less asymmetric toward longer wavelengths than the experimental one. The maximum of the simulated spectrum is also 2.6 nm redder, thus the Stokes shift between the calculated absorption and fluorescence spectra is a little exaggerated.

Figure 7 demonstrates the fluorescence emission lineshapes at three representative temperatures: 4.5 K (low temperature), 115 K (intermediate temperature), and 263 K (high temperature) together with their interpretation [thin solid lines, which represent the contribution of different exciton polaron states to the total modeled fluorescence emission spectrum (bold

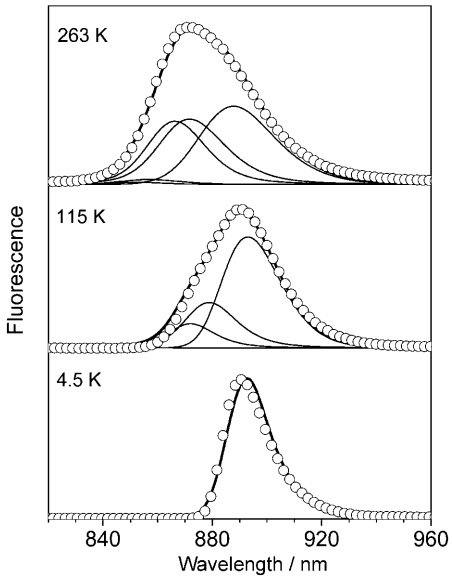

Figure 7. Experimental (scattered) and simulated (continuous lines) fluorescence emission lineshapes at three representative temperatures indicated. The contribution of different exciton polaron states is drawn with thin solid lines.

solid line)]. It can be seen that the major contributor to the temperature-dependent spectral shift and broadening is thermally assisted occupation of the higher-energy emitting states. Changes in line shapes are also visible but relatively minor.

Figure 6 summarizes the fitting results for the absorption and emission band positions (Figure 6a) and widths (Figure 6b) as a function of temperature. As seen, simulated data follow experiment fairly well, except the very highest temperatures. Accounting for likely temperature dependences of the inhomogeneous distribution functions would easily remedy also this shortage.

The simulation results for the anisotropy spectra at the three selected temperatures are shown in Figure 8. Due to high sensitivity with respect to the three-dimensional arrangement of the Bchl molecules in the protein scaffold, the dipole angles of Bchls in the LH2 complex have been adjusted within 2 degrees relative to them in the crystallographic structure. As a result, at all temperatures not only qualitative but almost quantitative reproduction of the measured spectra is achieved. Most importantly, the positions, widths, and depths of the anisotropy dips are successfully copied. Still, in correlation with other results, the fit becomes gradually poorer at higher temperatures, which only partly can be explained with diminishing spectral resolution.

In refs. [23, 29–31], the low-energy anisotropy minimum was assigned to the strongly absorbing exciton components with $k=\pm1$, and the high-energy minimum to the weak exciton components with $k=\pm8$. Here, we try to specify this assignment by switching off one-by-one the individual exciton states that contribute most into the simulated anisotropy spectra (Figure 9). For example, the solid thin line obtained by switching off the $k=\pm1$ states completely lacks the low-energy minimum at 862 nm. It is thus indeed clear that the $k=\pm1$ states largely contribute into the low-energy anisotropy dip. On the other hand, the high-energy anisotropy minimum appears to have more complex nature than assumed previously. Three, not just two states, contribute into this dip. As can be seen, it disappears from the spectrum only when the $k=\pm8$ and $k=9$ states are dropped out from the calculation. The complex origin of the high-energy minimum probably also explains its extra broadening when compared with the low-energy dip. It was also argued above that the energy gap, the energy difference between the high- and low-energy anisotropy minima, could be considered as a measure of the exciton bandwidth. One can see from Figure 4 that the experimental energy gap values position almost in the middle of the lines representing energy differences between the $k=0$ and $k=9$ and $k=\pm1$ and $k=\pm8$ exciton states. This justifies the operational definition applied previously[23,29–31] that the measured gap is approximately equal to the exciton bandwidth. The simulated

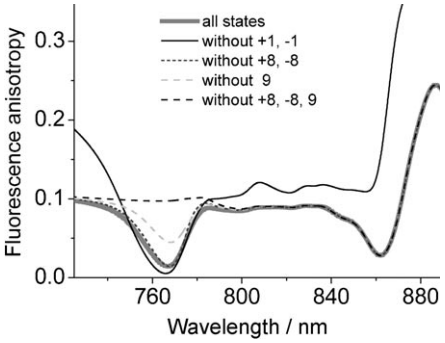

Figure 9. Simulated fluorescence anisotropy spectra at 5 K with different exciton states dropped out. Shown by continuous black, dotted, light gray and dark gray lines are the spectra that miss exciton states of $k=\pm1$, $k=\pm8$, $k=9$, and $k=\pm8$ and $k=9$, respectively. The reference curve with all 18 states included (the same as in Figure 8, lower curve) is drawn with bold gray line.

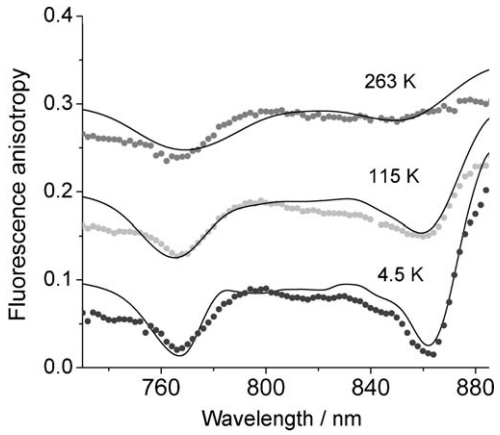

Figure 8. Experimental (scattered) and simulated fluorescence emission anisotropy spectra (solid lines) for LH2 complexes from *Rps. acidophila* at temperatures 4.5, 115, and 263 K. For better visibility, the middle and upper spectra are shifted vertically by 0.1 and 0.2 units, respectively.

gap values in Figure 4 coincide with the experimental data within experimental uncertainty.

3. Conclusions

The great advantage of biological samples like the B850 aggregate for model studies is that they consist of a small, fixed number of tightly packed molecules. Deeper comprehension of physics and chemistry of molecular materials (including biological matter) is available by means of investigations of similarities and/or differences between extended and discreet systems.

The theoretical approach applied herein accounts for physical differences in absorbing excitons in rigid and emitting exciton polarons in deformed antenna lattices. The idea of exciton polarons/self-trapped excitons in bacterial LH antennas has been around for at least a decade already.[23,34,49,50,52,53,66,67] Existence of similar quasi-localized excitations in DNA[68] as well as in photosynthetic reaction centers[13] has also been proposed recently. Successful reproduction of most subtle features of the measured spectra demonstrated above is another strong evidence for exciton polarons in the cyclic bacterial antennas.

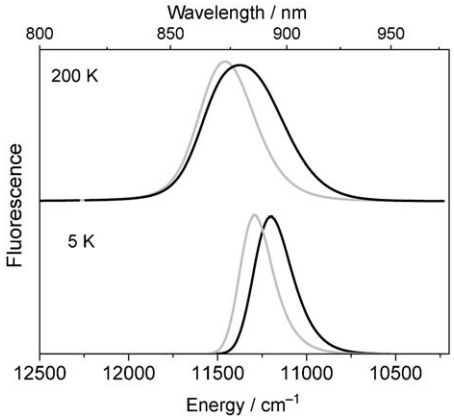

Figure 10. Simulated fluorescence emission spectra for LH2 complexes from *Rps. acidophila* according to Frenkel exciton (presented with gray line) and exciton polaron (black line) models. The spectra calculated at two indicated temperatures are normalized by peak intensity.

How essential the polaron coupling is for understanding the photophysical response of LH antenna excitations is demonstrated in Figure 10 (see also discussion in ref. [23]). Compared in Figure 10 at two temperatures are the fluorescence emission spectra simulated using either a Frenkel exciton model or the exciton polaron model in detail discussed herein. Both models possess the same diagonal exciton–phonon coupling energy, but only the exciton polaron model accounts for the off-diagonal coupling. All the calculation results of this work are based on the latter model.

As one can see from Figure 10, the fluorescence emission spectra of Frenkel excitons and exciton polarons at all temperatures significantly deviate from each other both in terms of the fluorescence band position and its shape. The relative peak shift equal to 90 cm^{-1} at 5 K can be considered as a direct consequence of inclusion of the off-diagonal reorganization energy (Table 1). The shape difference grows larger with temperature due to thermal occupation of the higher-energy states. Only the exiton polaron picture is in agreement with the experimental spectra.

Most of the other model parameters agree well with what has been published previously. At 100 K, the model predicts intra- and interdimer distances of 0.96 nm and 0.88 nm, respectively, in very good agreement with the 0.2 nm resolution crystal structure of [69]. The resulting intradimer couplings calculated in dipole–dipole approximation range from 374 cm^{-1} (5 K) to 322 cm^{-1} (300 K). Similar results obtained for interdimer couplings are 327 and 288 cm^{-1}. One may conclude a stronger effective exciton coupling strength (and a wider exciton bandwidth) in B850 aggregates from *Rps. acidophila* than in similar aggragtes from *Rb. sphaeroides*. This conclusion also corroborates with earlier data.[23,31] The site energy difference between α and β Bchls agrees with the number (300 cm^{-1}) found in ref. [70]. The exciton bandwidth, being one of the most important parameters of molecular excitons, is beyond resonance interactions also governed by diagonal and nondiagonal static and dynamic disorders operating in the system. Our model of phonon bath was verified by comparing with experimental low-temperature phonon sidebands of the line-narrowed fluorescence difference spectra.[52,53]

Herein, survival of excitons as collective, coherent quantum excitations with raising temperature in photosynthetic LH antenna nanoaggregates of purple bacteria is investigated. Apart from fundamental curiosity, this subject is generally important in order to connect the physical research done at cryogenic temperatures on various biological systems with their functioning at physiological temperatures. The essence of the problem is that quantum coherence requires the preservation of phase relationships.[11,26,45,71] Temperature, however, induces decoherence and dissipation of the coherent excitations that finally (at $k_BT > \Delta E$) would be expected to completely destroy the phase relationships and thus the excitons. The present experiments and their theoretical analyses unambiguously show survival of excitons in the whole studied temperature span, strongly suggesting that collective coherent electronic excitations play a role in the functional light-harvesting process. The exciton bandwidth in LH2 complexes from *Rps. acidophila*, for example, narrows only by 13%. Retrospectively (and qualitatively) speaking, this is a likely consequence of the strong exciton coupling of the LH2 antennas. The estimated nearest-neighbor exciton coupling energy between the Bchl molecules in the B850 aggregate of *Rps. acidophila* is much bigger than k_BT at ambient temperature (~205 cm^{-1}). Assuming no change of spatial geometry, the above decrease of exciton couplings between 5 and 300 K corresponds to about 0.05 nm increase of average distance between the neighbouring Bchl molecules, quite in line with the structural estimates.[72]

Experimental Section

Sample Preparation: Regular LH2 antenna complexes were isolated from chromatophores of the *Rps. acidophila* bacteria as described in ref. [73]. The samples stored at $-78\,^{\circ}C$ were before experiment diluted with the buffer–glycerol mixture (1:2 volume ratio) to yield a desired optical density in the sample cell (gelatine capsule of ~4 mm optical path length) and to obtain a good optical quality glass sample at low temperatures. The used 15 mM TEN buffer (pH 8.0) includes 3% LDAO. In fluorescence measurements the optical density in the sample cell measured in the peak of the Q_y absorption band was kept below 0.1, meaning that corrections for the fluorescence reabsorption were unnecessary. The sample was placed in a temperature-controlled He-bath cryostat (Utreks, Ukraine), where the temperature could be stabilized within ± 0.5 K between 4.5 and 300 K. The temperature was controlled with a calibrated silicon diode and a temperature monitor (Model 211, Lakeshore Cryotronics, USA).

Spectroscopy: Absorption and fluorescence emission spectra were recorded with the resolution of 0.4 nm using a 0.3 m spectrograph (Shamrock SR-303i, Andor Technology, UK) equipped with an electrically cooled CCD camera (model DV420A-OE, Andor Technology, UK). For absorption measurements, a high stability tungsten light source BPS100 (BWTek, USA) was employed. Selective excitation of fluorescence was carried out using a continuous-wave Ti:sapphire solid state laser (model 3900S, Spectra Physics, USA) with a line width less than 0.5 cm^{-1} pumped by an Ar-ion laser (model 171, Spectra Physics, USA). The conventional fluorescence spectra were excited at 450 nm with a light-emitting diode. The sample fluorescence was viewed in 90° geometry with respect to the excitation laser beam. The emitted light path was equipped with an analyzing polarizer, which direction was turned to either parallel or perpendicular with respect of vertically polarized excitation beam. The recorded fluorescence spectra were corrected for the wavelength sensitivity of the detection system. The fluorescence anisotropy spectrum was calculated according to Equation (14).

Spectral Fitting Procedures: The model relies on many parameters, some of which (such as the structural parameters of the complex, inhomogeneous distribution function of the lowest exciton polaron state, lifetime broadening of the exciton states, characteristics of the phonon modes, etc.) have certain experimental constraints.[23] The rest of the parameters were handled as "free" parameters. Numerical values of the latter parameters were found from fitting of the experimental spectra (fluorescence anisotropy, absorption and fluorescence peak positions, widths, etc.). First the theoretical spectra were generated with the Monte Carlo modeling, which then were compared with the experimental spectra applying nonlinear least squares fitting. To attain quick convergence the Levenberg–Marquard algorithm[74] was used, proven to be one of the best iterative algorithms for nonlinear fitting tasks. The algorithm has capability to converge even in case of ill-posed problems. To achieve a proper fit over the whole temperature range, temperature dependence of the complex size should be taken into account. The change of the complex linear dimensions for the α and β sub-lattices are modeled with an empirical sigmoid (19), being justified by the previous research:[36,40]

$$R_{\beta}^{\alpha}(T) = R_{\beta}^{\alpha}(0)\left[A + \frac{B}{\exp\left(-\frac{T-C}{D}\right)+1}\right] \qquad (19)$$

In Equation (19), $R_{\beta}^{\alpha}(0)$ is the corresponding radius given in ref. [58].

Acknowledgements

This work was partially supported by the Estonian Science Foundation (grant No. 8674), the Estonian Ministry of Education and Science (grant No. SF0180055s07), and the Research Council of Lithuania (grant No. MIP-110/2010). We are grateful to T. Gillbro for kindly presenting the LH2 samples from Rps. acidophila.

Keywords: excitons · fluorescence · nano-aggregates · photochemistry · photosynthetic light harvesting

[1] M. Kasha, *Radiat. Res.* **1963**, *20*, 55–71.
[2] M.-H. Whangbo, *Acc. Chem. Res.* **1983**, *16*, 95–101.
[3] T. Markvart, *Prog. Quantum Electron.* **2000**, *24*, 107–186.
[4] G. D. Scholes, G. Rumbles, *Nat. Mater.* **2006**, *5*, 683–693.
[5] F. C. Spano, *Annu. Rev. Phys. Chem.* **2006**, *57*, 217–243.
[6] D. Beljonne, C. Curutchet, G. D. Scholes, R. J. Silbey, *J. Phys. Chem. B* **2009**, *113*, 6583–6599.
[7] D. Abramavicius, B. Palmieri, D. V. Voronine, F. Sanda, S. Mukamel, *Chem. Rev.* **2009**, *109*, 2350–2408.
[8] F. C. Spano, *Acc. Chem. Res.* **2010**, *43*, 429–439.
[9] R. E. Blankenship, *Molecular Mechanisms of Photosynthesis*, Blackwell, Oxford, **2002**.
[10] Z. G. Fetisova, A. Freiberg, K. Timpmann, *Nature* **1988**, *334*, 633–634.
[11] H. Van Amerongen, L. Valkunas, R. Van Grondelle, *Photosynthetic Excitons*, World Scientific, Singapore, **2000**.
[12] T. S. Balaban, *FEBS Lett.* **2003**, *545*, 97–102.
[13] R. A. Khatypov, A. Y. Khmelnitskiy, M. M. Leonova, L. G. Vasilieva, V. A. Shuvalov, *Photosynth. Res.* **2008**, *98*, 81–93.
[14] X. Hu, T. Ritz, A. Damjanovic, F. Autenrieth, K. Schulten, *Q. Rev. Biophys.* **2002**, *35*, 1–62.
[15] R. J. Cogdell, A. Gall, J. Köhler, *Q. Rev. Biophys.* **2006**, *39*, 227–324.
[16] A. Y. Borisov, A. M. Freiberg, V. I. Godik, K. Rebane, K. Timpmann, *Biochim. Biophys. Acta Bioenerg.* **1985**, *807*, 221–229.
[17] K. Timpmann, A. Freiberg, V. I. Godik, *Chem. Phys. Lett.* **1991**, *182*, 617–622.
[18] K. Timpmann, N. W. Woodbury, A. Freiberg, *J. Phys. Chem. B* **2000**, *104*, 9769–9771.
[19] A. Freiberg, J. P. Allen, J. Williams, N. W. Woodbury, *Photosynth. Res.* **1996**, *48*, 309–319.
[20] M. Sener, J. Strümpfer, J. A. Timney, A. Freiberg, C. N. Hunter, K. Schulten, *Biophys. J.* **2010**, *99*, 67–75.
[21] V. Sundström, T. Pullerits, R. van Grondelle, *J. Phys. Chem. B* **1999**, *103*, 2327–2346.
[22] R. Van Grondelle, V. I. Novoderezhkin, *Phys. Chem. Chem. Phys.* **2006**, *8*, 793–807.
[23] A. Freiberg, G. Trinkunas in *Unraveling the hidden nature of antenna excitations* (Eds.: A. Laisk, L. Nedbal, Govindjee), Springer, Heidelberg, **2009**, pp. 55–82.
[24] A. Freiberg, K. Timpmann, R. Ruus, N. W. Woodbury, *J. Phys. Chem. B* **1999**, *103*, 10032–10041.
[25] V. Liuolia, L. Valkunas, R. van Grondelle, *J. Phys. Chem. B* **1997**, *101*, 7343–7349.
[26] A. S. Davydov, *Theory of Molecular Excitons*, Plenum, New York, **1971**.
[27] G. McDermott, S. M. Prince, A. A. Freer, A. M. Hawthornthwaite-Lawless, M. Z. Papiz, R. J. Cogdell, N. W. Isaacs, *Nature* **1995**, *374*, 517–521.
[28] M. Rätsep, C. N. Hunter, J. D. Olsen, A. Freiberg, *Photosynth. Res.* **2005**, *86*, 37–48.
[29] K. Timpmann, G. Trinkunas, J. D. Olsen, C. N. Hunter, A. Freiberg, *Chem. Phys. Lett.* **2004**, *398*, 384–388.
[30] K. Timpmann, G. Trinkunas, P. Qian, C. N. Hunter, A. Freiberg, *Chem. Phys. Lett.* **2005**, *414*, 359–363.
[31] A. Freiberg, K. Timpmann, G. Trinkunas, *Chem. Phys. Lett.* **2010**, *500*, 111–115.
[32] A. Gall, E. Sogaila, V. Gulbinas, O. Ilioaia, B. Robert, L. Valkunas, *Biochim. Biophys. Acta Bioenerg.* **2010**, *1797*, 1465–1469.

[33] R. Monshouwer, M. Abrahamsson, F. van Mourik, R. van Grondelle, *J. Phys. Chem. B* **1997**, *101*, 7241 – 7248.
[34] A. Freiberg, M. Rätsep, K. Timpmann, G. Trinkunas, N. W. Woodbury, *J. Phys. Chem. B* **2003**, *107*, 11510 – 11519.
[35] V. Urboniene, O. Vrublevskaja, G. Trinkunas, A. Gall, B. Robert, L. Valkunas, *Biophys. J.* **2007**, *93*, 2188 – 2198.
[36] H.-M. Wu, M. Rätsep, R. Jankowiak, R. J. Cogdell, G. J. Small, *J. Phys. Chem. B* **1997**, *101*, 7641 – 7653.
[37] O. Zerlauskiene, G. Trinkunas, A. Gall, B. Robert, V. Urboniene, L. Valkunas, *J. Phys. Chem. B* **2008**, *112*, 15883 – 15892.
[38] Y. Zhao, T. Meier, W. M. Zhang, V. Chernyak, S. Mukamel, *J. Phys. Chem. B* **1999**, *103*, 3954 – 3962.
[39] A. Freiberg, K. Timpmann, S. Lin, N. W. Woodbury, *J. Phys. Chem. B* **1998**, *102*, 10974 – 10982.
[40] K. Timpmann, A. Ellervee, A. Kuznetsov, A. Laisaar, G. Trinkunas, A. Freiberg, *J. Lumin.* **2003**, *102–103*, 220 – 225.
[41] R. E. Merrifield, *J. Chem. Phys.* **1964**, *40*, 445 – 450.
[42] T. Holstein, *Ann. Phys.* **1959**, *8*, 325 – 342.
[43] I. E. Rashba in *Self-trapping of excitons*. (Ed.: M. D. Sturge), North-Holland, Amsterdam, **1982**, pp. 543 – 602.
[44] D. Emin, T. Holstein, *Phys. Rev. Lett.* **1976**, *36*, 323 – 326.
[45] Y. Toyozawa, *Optical Processes in Solids*, Cambridge University Press, Cambridge, **2003**.
[46] D. Leupold, H. Stiel, K. Teuchner, F. Nowak, W. Sandner, B. Uecker, H. Scheer, *Phys. Rev. Lett.* **1996**, *77*, 4675 – 4678.
[47] O. Kühn, V. Sundstrom, *J. Chem. Phys.* **1997**, *107*, 4154 – 4164.
[48] L. D. Book, A. E. Ostafin, N. Ponomarenko, J. R. Norris, N. F. Scherer, *J. Phys. Chem. B* **2000**, *104*, 8295 – 8307.
[49] T. Polivka, T. Pullerits, J. L. Herek, V. Sundström, *J. Phys. Chem. B* **2000**, *104*, 1088 – 1096.
[50] K. Timpmann, Z. Katiliene, N. W. Woodbury, A. Freiberg, *J. Phys. Chem. B* **2001**, *105*, 12223 – 12225.
[51] A. Damjanovic, I. Kosztin, U. Kleinekathöfer, K. Schulten, *Phys. Rev. E* **2002**, *65*, 031 919 – 031 943.
[52] K. Timpmann, M. Rätsep, C. N. Hunter, A. Freiberg, *J. Phys. Chem. B* **2004**, *108*, 10581 – 10588.
[53] A. Freiberg, M. Rätsep, K. Timpmann, G. Trinkunas, *Chem. Phys.* **2009**, *357*, 102 – 112.
[54] G. Trinkunas, A. Freiberg, *J. Lumin.* **2005**, *112*, 420 – 423.
[55] G. Trinkunas, A. Freiberg, *J. Lumin.* **2006**, *119–120*, 105 – 110.
[56] T. Meier, Y. Zhao, V. Chernyak, S. Mukamel, *J. Chem. Phys.* **1997**, *107*, 3876 – 3893.
[57] A. J. Heeger, S. Kivelson, J. R. Schrieffer, W.-P. Su, *Rev. Mod. Phys.* **1988**, *60*, 781 – 851.
[58] S. Jang, R. J. Silbey, *J. Chem. Phys.* **2003**, *118*, 9324 – 9336.
[59] H. Fidder, J. Knoester, D. A. Wiersma, *J. Chem. Phys.* **1991**, *95*, 7880 – 7890.
[60] S. Mukamel, *Principles of Nonlinear Optical Spectroscopy*, Oxford University Press, New York, **1995**.
[61] M. Rätsep, A. Freiberg, *Chem. Phys. Lett.* **2003**, *377*, 371 – 376.
[62] S. Jang, J. Cao, R. J. Silbey, *J. Phys. Chem. B* **2002**, *106*, 8313 – 8317.
[63] R. Agarwal, A. H. Rizvi, B. S. Prall, J. D. Olsen, C. N. Hunter, G. R. Fleming, *J. Phys. Chem. A* **2002**, *106*, 7573 – 7578.
[64] K. Noba, Y. Kayanuma, *J. Phys. Soc. Jpn.* **1998**, *67*, 3972 – 3975.
[65] J. R. Lakowicz, *Principles of Fluorescence Spectroscopy*, Plenum, New York, **1983**.
[66] A. Freiberg, M. Rätsep, K. Timpmann, G. Trinkunas, *J. Lumin.* **2003**, *102–103*, 363 – 368.
[67] A. Freiberg, M. Rätsep, K. Timpmann, G. Trinkunas, *J. Lumin.* **2004**, *108*, 107 – 110.
[68] C. T. Middleton, K. de La Harpe, C. Su, Y. K. Law, C. E. Crespo-Hernandez, B. Kohler, *Annu. Rev. Phys. Chem.* **2009**, *60*, 217 – 239.
[69] M. Z. Papiz, S. M. Prince, T. Howard, R. J. Cogdell, N. W. Isaacs, *J. Mol. Biol.* **2003**, *326*, 1523 – 1538.
[70] M. H. C. Koolhaas, R. N. Frese, G. J. S. Fowler, T. A. Bibby, S. Georgakopoulou, G. v. d. Zwan, C. N. Hunter, R. van Grondelle, *Biochemistry* **1998**, *37*, 4693 – 4698.
[71] C. B. Harris, D. A. Zwemer, *Annu. Rev. Phys. Chem.* **1978**, *29*, 473 – 495.
[72] M. Z. Papiz, S. M. Prince, T. Howard, R. J. Cogdell, N. W. Isaacs, *J. Mol. Biol.* **2003**, *326*, 1523 – 1538.
[73] Y.-Z. Ma, R. J. Cogdell, T. Gillbro, *J. Phys. Chem. B* **1997**, *101*, 1087 – 1095.
[74] K. Levenberg, *Q. Appl. Math.* **1944**, *2*, 164 – 168.

Received: October 31, 2010
Published online on January 27, 2011

